 doi:10.20944/preprints201812.0139.v1

Article

Characterizing selected wetland habitats' desiccation phenomena using the Crop Water Stress Index

Maciej Góraj [1]*, Wojciech Ciężkowski [1], Piotr Sikorski [2], Małgorzata Kleniewska [1], Sylwia Szporak-Wasilewska [3], Jacek Jóźwiak [1], Tomasz Gnatowski [4], Jan Szatyłowicz [4], Jarosław Chormański [1]

[1] Department of Hydraulic Engineering, Faculty of Civil and Environmental Engineering, Warsaw University of Life Sciences - SGGW, Nowoursynowska 166, 02-787 Warsaw, Poland; m.goraj@levis.sggw.pl (M.G.), w.ciezkowski@levis.sggw.pl (W.C), malgorzata_kleniewska@sggw.pl (M.K.); j.jozwiak@levis.sggw.pl (J.J.), j.chormanski@levis.sggw.pl (J.C.);
[2] Department of Environmental Protection, Faculty of Horticulture and Landscape Architecture, Warsaw University of Life Sciences - SGGW, Nowoursynowska 166, 02-787 Warsaw, Poland; piotr_sikorski@sggw.pl
[3] Water Center Laboratory, Faculty of Civil and Environmental Engineering, Warsaw University of Life Sciences - SGGW, Nowoursynowska 166, 02-787 Warsaw, Poland; s-szporak@levis.sggw.pl
[4] Department of Environmental Improvement, Faculty of Civil and Environmental Engineering, Warsaw University of Life Sciences - SGGW, Nowoursynowska 166, 02-787 Warsaw, Poland; tomasz_gnatowski@sggw.pl (T.G.), piotr_dabrowski@sggw.pl (P.D.), jan_szatylowicz@sggw.pl (J.S.)
* Correspondence: m.goraj@levis.sggw.pl; Tel.: +48-22-593-53-07

Abstract: The research carried out concerned the laboratory assessment of the applicability of the Crop Water Stress Index (CWSI) as a practical tool for assessing the risk of desiccation for selected wetland habitats: transition mires and quaking bogs as well as alkaline fens. The analysis was carried out on 3 soil samples with a vegetation cover (with the dimensions of 40×40×30 cm) collected during the full vegetation season for each mentioned habitat, with a characteristic species composition. Experimental research was carried out between 17th May 2018 and 19th June 2018. Thermal, RGB and multispectral images, chlorophyll content, volumetric soil moisture, air temperature and relative humidity measurements were taken for each sample every two days. The obtained results clearly indicate the dependence between CWSI and plant condition parameters in the first phase of desiccation. At the same time, as a result of the observations taken, thresholds have been set, indicating different desiccation phases.

Keywords: drought, water management, thermal remote sensing, habitats protection, land surface temperature, CWSI

1. Introduction

Soil drought is a state of water deficit in the root zone of plants. This condition constitutes a factor limiting plant growth [1]. In the case of organic soils, such as peats building valuable wetland habitats, the occurrence of long-lasting soil drought episodes contributes to the permanent change of the physical properties of the organic soils and consequently succession changes in wetland habitats. The long-term lowering of the groundwater table leads to: the consolidation process [2],an acceleration of the mineralization of organic matter, and as a consequence, to an increase in the emission of gaseous decomposition products, such as carbon dioxide. This phenomenon was described by various authors, including [3-5].

Another threat to valuable wetland habitats resulting from a long-term drought period is the change in habitat conditions, e.g. volumetric soil moisture, and consequently, the disturbance of the existing dominance structure of species composition in the plant communities inhabiting a given patch [6,7]. In a drastic case, it is even possible for the present habitat to transform into another, more

xerophilic one [8]. In connection with the change of habitat conditions prevailing within a given patch, there is also a threat of entry of alien species [9].

By 2100, the frequency of droughts in Europe is expected to increase. The largest increase relates to summer droughts as well as autumn and spring droughts in southern Europe and the Iberian Peninsula. However, the increase in the frequency of droughts throughout the year is expected to take place all over Europe [10]. Up to 2050, an increase in the deficit of precipitation and, consequently, the frequency and magnitude of droughts is forecasted [11].

Due to the growing risk of drought, there is a need to develop indicators allowing to identify areas exposed to degradation resulting from the particular intensity of this phenomenon [12]. As a consequence, numerous indices have been developed in order to detect and quantify the phenomenon of drought. The most popular include meteorological drought indicators like: Standardized Precipitation Index [13-16], Relative Precipitation Index [17], Effective Drought Index [18-20], Climatic Water Balance [12], Standardized Climatic Water Balance [21] and soil drought indicators like: the Soil Moisture Index [22,23] or the Crop Water Stress Index [24,25].

The Crop Water Stress Index (CWSI) has gained significant popularity due to its practical implementation in agriculture. It is an index with wide possibilities in this field, used to assess the needs of irrigation on agricultural and horticultural crops, and at the same time this index has been examined in detail in regard to, cereal crops [26, 27], soy [28, 29], vegetables [30, 31], sugar beet [32], grapes [33], or olive and fruit trees [34, 35] among others. In order to carry out calculations, this index requires measurements of i.a. land surface temperature (LST), which based on thermal infrared imaging (TIR), is currently one of the dynamically developed technologies. Its development involves the use of thermal sensors mounted on various platforms operating on the satellite [28], airborne [36] and UAV ceiling [33, 35, 37].

Agricultural areas are well recognized for the use of CWSI, including the dependence of the index value and the observed drying risk levels [26, 28, 30]. However, these are usually monocultural habitats with little water stress flexibility. On the other hand, there is a lack of research on habitats with heterogeneous species composition, such as natural habitats, including wetland habitats. It can be presumed that in this case, the reaction of plants subjected to the stress factor will be inhomogeneous in space, dependent on the local species composition and the structure of domination. Plant species in wetland habitats, characterized by a shallow location of the groundwater table even in drought conditions, may react differently to a periodic water shortage. In this case, CWSI during the shortage period will have a different course for each plant species and could be hard to interpret.

The aim of the study presented in this paper is to examine the course of CWSI values as a response to water stress of natural habitats with high and distinct species diversity, developed on organic soils with high sensitivity to water content reduction. Transition mires and quaking bogs and alkaline fens were selected for the analysis. Firstly, representative soil samples together with covering vegetation were extracted from each of the habitats and transported to the laboratory. Secondly, soil moisture changes in time occurring as a result of evapotranspiration were observed for each sample during one month along with measurements of meteorological parameters and plant condition indices for detection of physiological changes. Thermal and RGB images were simultaneously acquired.

2. Materials and Methods

2.1. CWSI, the basics and limitations of the method

CWSI (the value ranges from -1 to 1) is determined on the basis of measurements of the surface temperature of plants and basic meteorological parameters (temperature and relative humidity of the air). For its calculation, it is necessary to determine the non-water stress baseline (NWSB) for the examined habitats, which is a linear relationship that exists between vegetation-air temperature differential and air vapor pressure deficit (VPD) for plants in optimal water conditions [38].

 doi:10.20944/preprints201812.0139.v1

$$dT=a\cdot VPD+b, \quad (1)$$

Knowing the parameters a and b (linear equation parameters) of the NWSB, CWSI is calculated using the following formula:

$$CWSI=(dT_m-dT_{LL})/(dT_{UL}-dT_{LL}), \quad (2)$$

where: dT – difference between the temperature of vegetation and air, subscripts: m, LL and UL refer to the measured, lower and upper dT limit respectively. dT_{LL} and dT_{UL} are calculated from the following formulas [39]:

$$dT_{LL}=a\cdot VPD+b, \quad (3)$$

$$dT_{UL}=a\cdot VPG+b, \quad (4)$$

where: VPD (KPa) – air vapor pressure deficit, VPG (KPa) – air vapor pressure gradient determined as the difference between the saturation water vapor pressure at a given air temperature and the saturation water vapor pressure at an air temperature elevated by the coefficient "b".

In this study NWSB for transition mires and quaking bogs: dT=-7.42·VPD+16.3, and for alkaline fens: dT=-11.63·VPD+21.3 determined by [40] are used. The measurements necessary to determine the CWSI should take place in proper meteorological conditions, such as: wind speed bellow 5 m·s-1, clear sky and high air temperature (above 20 °C) [33, 41].

2.2. Assumptions of the experiment

It was assumed that the experiment will allow to determine desiccation thresholds due to water shortage by continuous observation of changes in CWSI values, habitat condition indicators such as soil moisture and chlorophyll content and plant species composition. On their basis, it is possible to determine the range of the index value, in which the habitat is in optimal soil moisture conditions, as well as the period when the habitat begins to dry out due to water shortage (initial drying phase) and the moment when the habitat is dried up due to a longer period of water shortage.

2.3. Sampling

For the purposes of the experiment, samples of transition mires and quaking bogs and alkaline fens were collected in triplicate. Each habitat sample was characterized by a different species composition, which was typical for the examined habitats. This allowed the analysis of the impact of local species composition on the CWSI.

Coverage of each plant genus was evaluated in the field using the geobotanical method [42] under optimal soil moisture conditions before sampling. The plant species with their frequency are shown in Table A1.

The samples of transition mires and quaking bogs were extracted in Lasy Janowskie Landscape Park on two overgrown ponds (Figure 1A) with the domination of *Eriophorum angustifolium* (L1), *Carex lasiocarpa* with *Oxycoccus palustris* (L2) and *Carex lasiocarpa* (L3). The samples of alkaline fens were extracted in Biebrza National Park (Figure 1B) with the domination of *Menyanthes trifoliata* with low participation of mosses (B1, B3) and *Carex rostrata* (B2).

 doi:10.20944/preprints201812.0139.v1

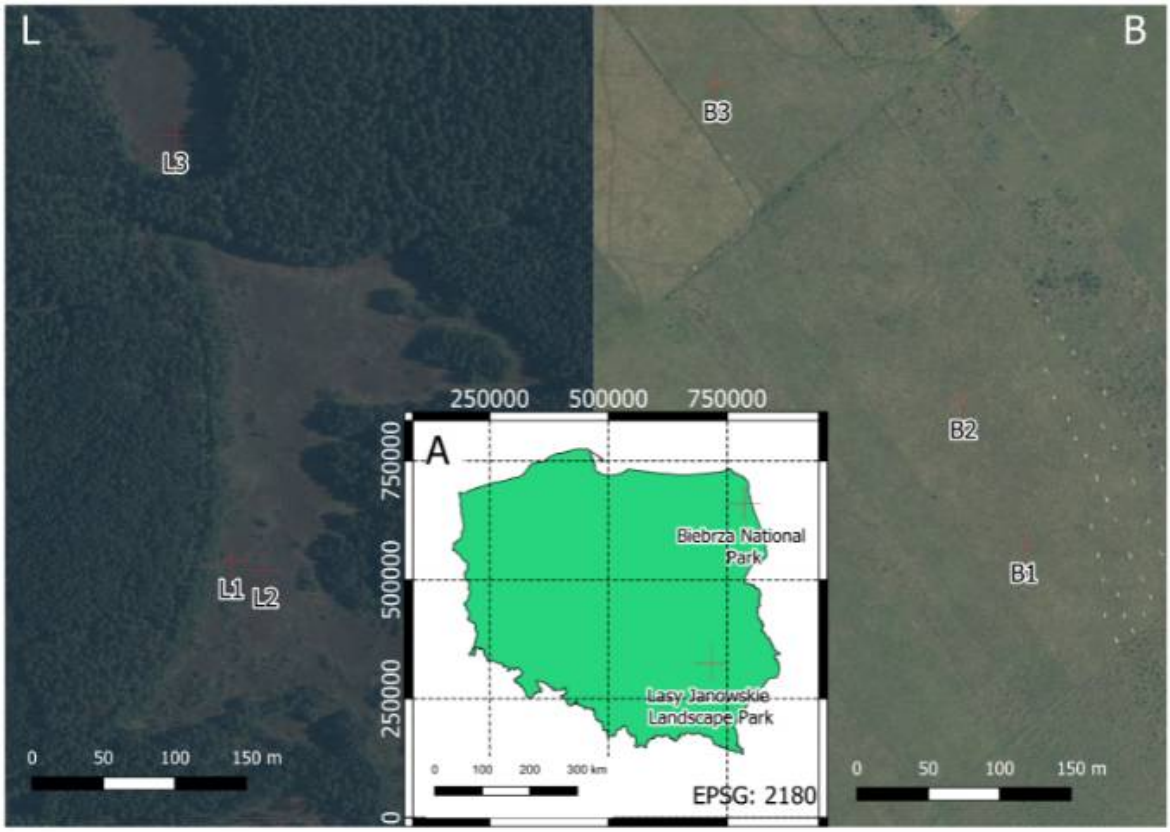

Figure 1. Location of research areas in Poland (**A**) and sample sites in Lasy Janowskie Landscape Park (**L**) - (coordinates of L1: 716013.630E, 324183.511N) and Biebrza National Park (**B**) - (B1: 786030.925E, 660308.047N)

The collected peat samples with a square size of 40×40 cm and a depth of 30 cm were transferred to a laboratory, where they were stored under controlled conditions. After transporting, the samples were supplied with water taken from the parent area and then maintained with no access to precipitation. In this way, the process of long-term drying of the analyzed habitats was simulated. Additionally, soil samples were taken to determine full water capacity (θ_s).

2.4. Course of the experiment

The experimental research was carried out between 17th May 2018 and 19th June 2018. The following observations were carried out during the experiment:

- Volumetric soil moisture (VSM)
- Air temperature (AT)
- Relative humidity (RH)
- Chlorophyll content (CC)
- Description of botanical composition (BC)
- Visible imaging (RGB)
- Multispectral imaging (MS)
- Thermal imaging (land surface temperature, LST)

Based on observations following indicators were prepared:

- Crop Water Stress Index (CWSI)
- Percentage of living plants (PLP)
- Normalized Difference Vegetation Index (NDVI)
- Desiccation thresholds (DT)
- Critical volumetric soil moisture (VSMC).

Meteorological parameters (AT, RH) were measured continuously using the HOBO U23 Pro v2 Temperature/Relative Moisture Data Logger sensor (Onset®, USA), which was placed at a height of

Preprints (www.preprints.org) | NOT PEER-REVIEWED | Posted: 12 December 2018 doi:10.20944/preprints201812.0139.v1

2 m in a cover protecting it from direct radiation and precipitation. The sensor recorded data with a 10-minute time step. The rest of the listed parameters were measured once per two days.

The weight method was used to estimate VSM. The assumption was made that the change in the mass of the sample corresponds to the change in the VSM. The initial VSM, measured after the filling the sample with water was considered to be equal to the s.

For each sample CC was observed for up to 3 species characterized by the biggest coverage. Observations were performed in the 16 square elementary areas (Figure 2) with a side of 10 cm. The CCM-300 (Opti-sciences, inc., USA) instrument was used to measure the chlorophyll content (CC).

(**a**)

Figure 2. An exemplary square grid (red net) used in the experiment (RGB image of L2 sample)

At the beginning and at the end of experiment botanical composition was determined by a botanist. The species layers and coverage were determined (shown in Table A1).

RGB and MS imaging were performed using Sequoia camera (Parrot Drones, SAS, France) placed on the fixed height equal to 1.5 m above the sample surface. On the basis of visual analysis of RGB images, a base of reference polygons was created, which was then used to classify images. The Maximum Likelihood classifier was used [43]. In this way, pixels representing living and dry parts of plants were identified (PLP). The classification was performed based reference polygons (classes: living plants, dried plants, background) were split into training and validation subpopulations. Results characterized by kappa not less than 0.8 were included for further analyses.

Based on MS images NDVI was calculated for selected dates according to formula 5.

$$NDVI=(NIR-RED)/(NIR+RED), \quad (5)$$

where: NIR - near-infrared brightness, RED - red brightness.

The LST was measured using the PI640 thermal camera (Optris, GmbH, Germany) at the fixed height equal to 1.5 m above the sample surface. Using mean LST for each elementary area as well as AT and RH, based on 1-4 formulas, NWSB and further CWSI was determined.

Based on the results of VSM, CC, BC, RGB and MS observations the desiccation thresholds (DT) were determined for each of the six samples based on trend analysis of the described features.

3. Results

The first part of the chapter presents the dynamics of the observed quantities (VSM, CWSI, CC, BC, PLP, NDVI) along with their analysis. The next part presents the methodology for determining the desiccation threshold (DT) and desiccation phases.

3.1. VSM

During the experiment, VSM in habitat alkaline fens decreases from the level of approximately 0.90 $m^3 * m^{-3}$ to approx. 0.50-0.60 $m^3 * m^{-3}$, 16.0 – 18.5 kg loss of weight (Figure 3). VSM in transition mires and quaking bogs decreases from the level of approx. 0.95 $m^3 * m^{-3}$ to approx. 0.65-0.70 $m^3 * m^{-}$

Preprints (www.preprints.org) | NOT PEER-REVIEWED | Posted: 12 December 2018 doi:10.20944/preprints201812.0139.v1

^{3}, 10.5 – 13.55 kg loss of weight (Figure 3). A clearly outlying value of VSM was observed in the case of sample L3, which was collected from the smaller northern pond, more exposed to fluctuations in the groundwater table (Figure 3).

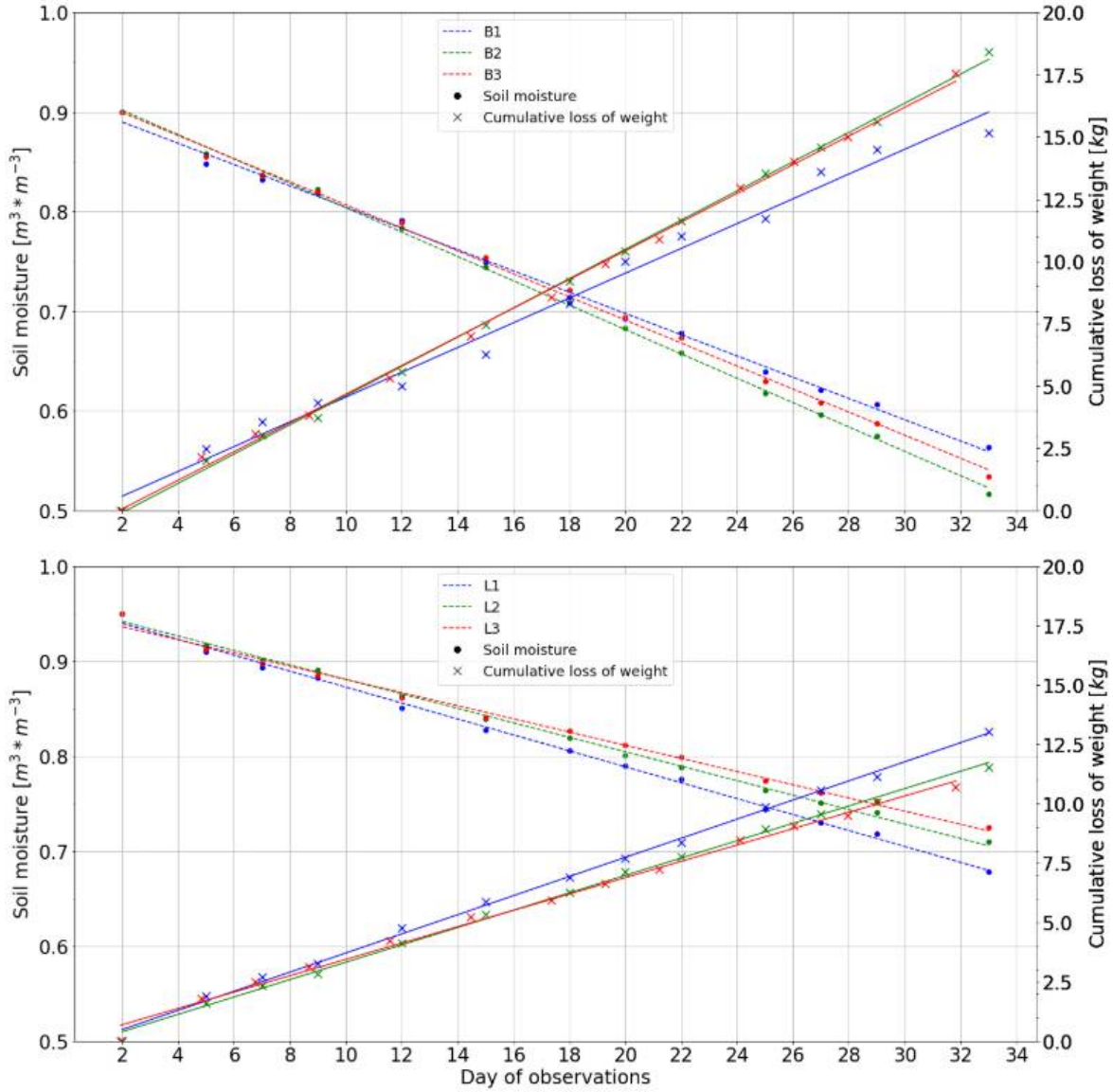

Figure 3. The Cumulative loss of weight and VSM dynamics in alkaline fens (**top panel**) and transition mires and quaking bogs (**bottom panel**) habitat samples.

3.2. CWSI

The CWSI dynamics were presented in the form of a box plot for 16 elementary areas. For transition mires and quaking bogs, the CWSI dynamics are similar for samples L1 and L2, which were collected on the southern pond. A change from approx. -0.3 (good moisture condition) to ca. 0.2 (drying state) is observed. Sample 3 changes from -0.2 (good moisture condition) to ca. 0.19 (drying state) (Figure 4).

The CWSI dynamics for alkaline fens is similar for each of the analyzed samples. A change from ca. -0.18 (good moisture condition) to ca. 0.15 (drying state) is observed (Figure 4).

Preprints (www.preprints.org) | NOT PEER-REVIEWED | Posted: 12 December 2018 doi:10.20944/preprints201812.0139.v1

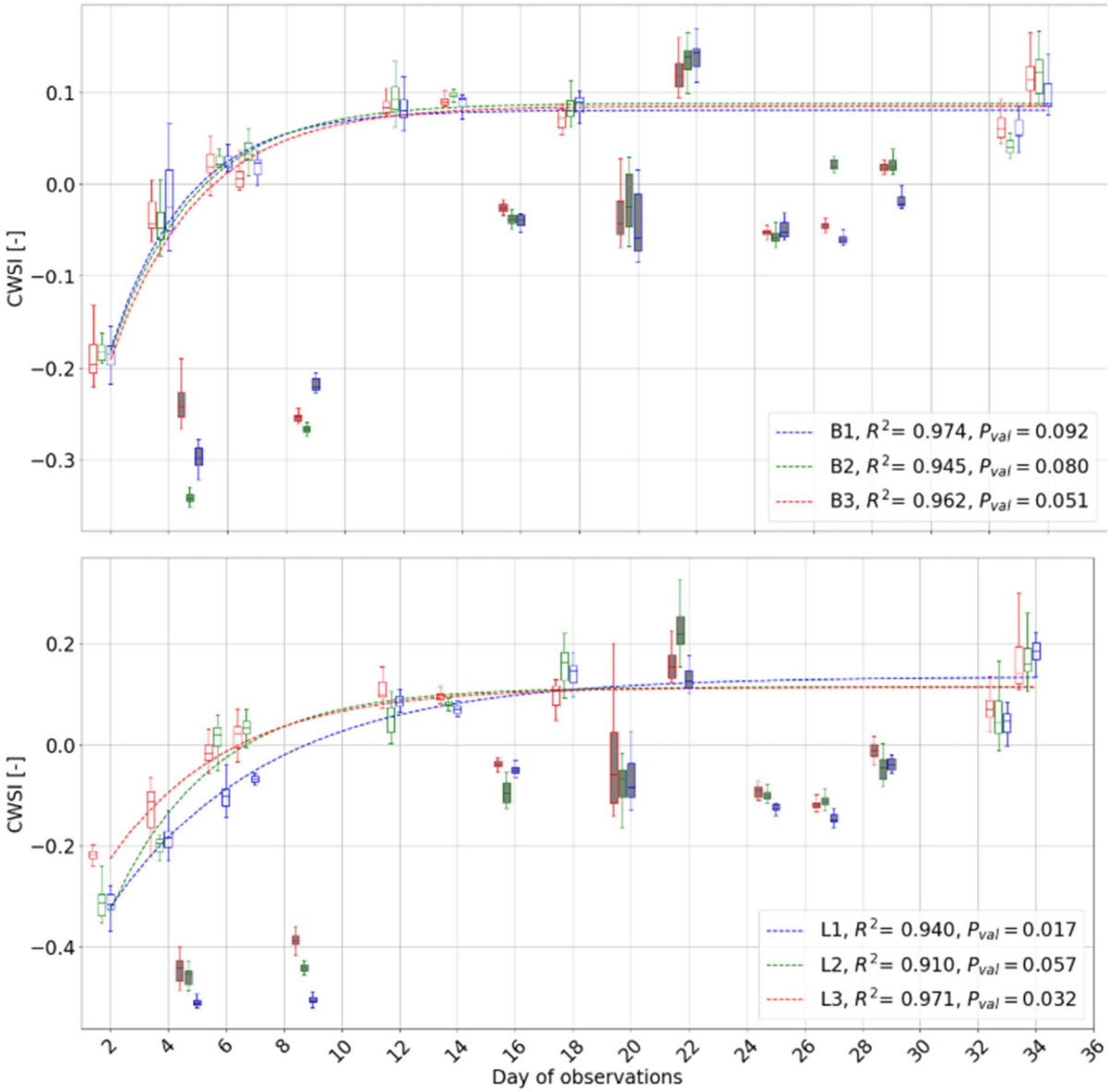

Figure 4. The CWSI dynamics observed in alkaline fens (**top panel**) and transition mires and quaking bogs (**bottom panel**) habitat samples. Boxes present CWSI measured in 16 elementary areas. Gray boxes represent CWSI observed on cloudy days (they were rejected from the population used for trend analysis due to improper conditions during the observation). Box edges show 25th and 75th quartile, horizontal line inside the box shows median, whiskers and caps shows all others non-outlier data points.

3.3. CC

The CC dynamics were presented in the form of a box plot from 16 elementary areas for both herbaceous layers (Figure 5) and mosses (Figure 6).

During the experiment, the mean CC measured for both vegetation layers in transition mires and quaking bogs decreased by 20 mg * m^{-2} for samples 2 and 3, while the decrease of this value was lower in the case of sample 1, amounting to approx. 10 mg * m^{-2} (Figure 5).

In turn, the average CC measured for both vegetation layers in alkaline fens decreased by 15 mg * m^{-2} for samples 1 and 3. In the first part of the experiment (until the 19th day of observations) in the case of sample 2, a decrease by 20 mg * m^{-2} is visible, followed by an increase related to the development of *Filipendula ulmaria*. This species began colonizing the sample around 22th day of observations and caused an increase in the average CC for the sample up to the level of approx. 230 mg * m^{-2}. The most visible decrease of CC was observed in mosses layer (Figure 5).

Preprints (www.preprints.org) | NOT PEER-REVIEWED | Posted: 12 December 2018 doi:10.20944/preprints201812.0139.v1

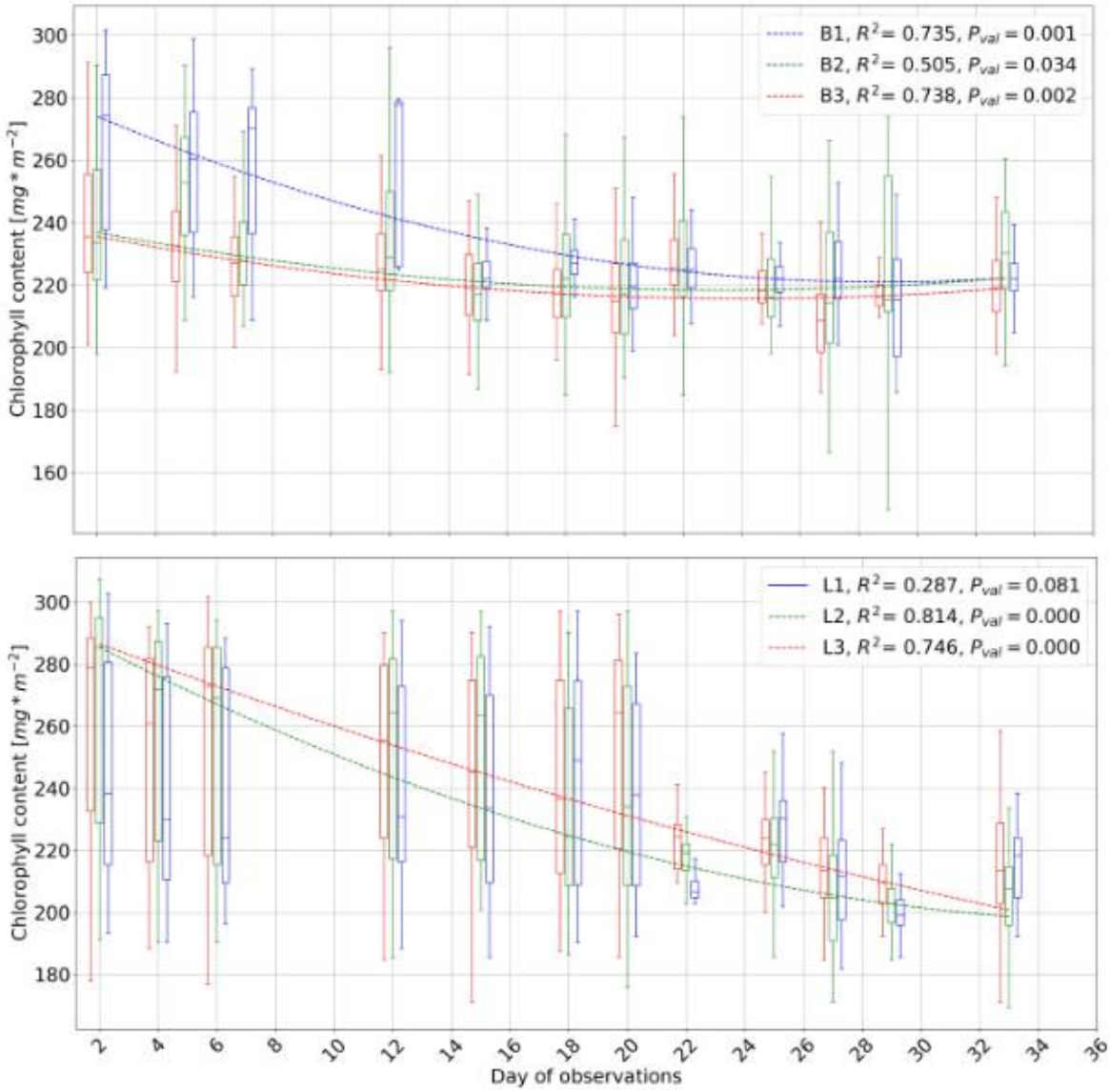

Figure 5. The CC dynamics observed in alkaline fens (**top panel**) and transition mires and quaking bogs (**bottom panel**) habitat samples for both mosses and herbaceous layers. Boxes present CC measured for all observed species in mosses and herbaceous layers in 16 elementary areas. Box edges show 25th and 75th quartile, horizontal line inside the box shows median, whiskers and caps shows all others non-outlier data points.

During the experiment, the most visible decrease of CC was observed in case of mosses layer (Figure 6). The CC for alkaline fens was possible to observe until the 12th day of the experiment, during which continuous decrease is visible (Figure6). After 12th day gained signal was too weak to registrate CC. In turn, for transition mires and quaking bogs, CC was decreasing slowly until the 10th day of observations. After the 10th day, the abrupt reduction of the value was observed. Starting on the 20th day of observations, the signal gain of CC was outside the device range (Figure 6).

Preprints (www.preprints.org) | NOT PEER-REVIEWED | Posted: 12 December 2018 doi:10.20944/preprints201812.0139.v1

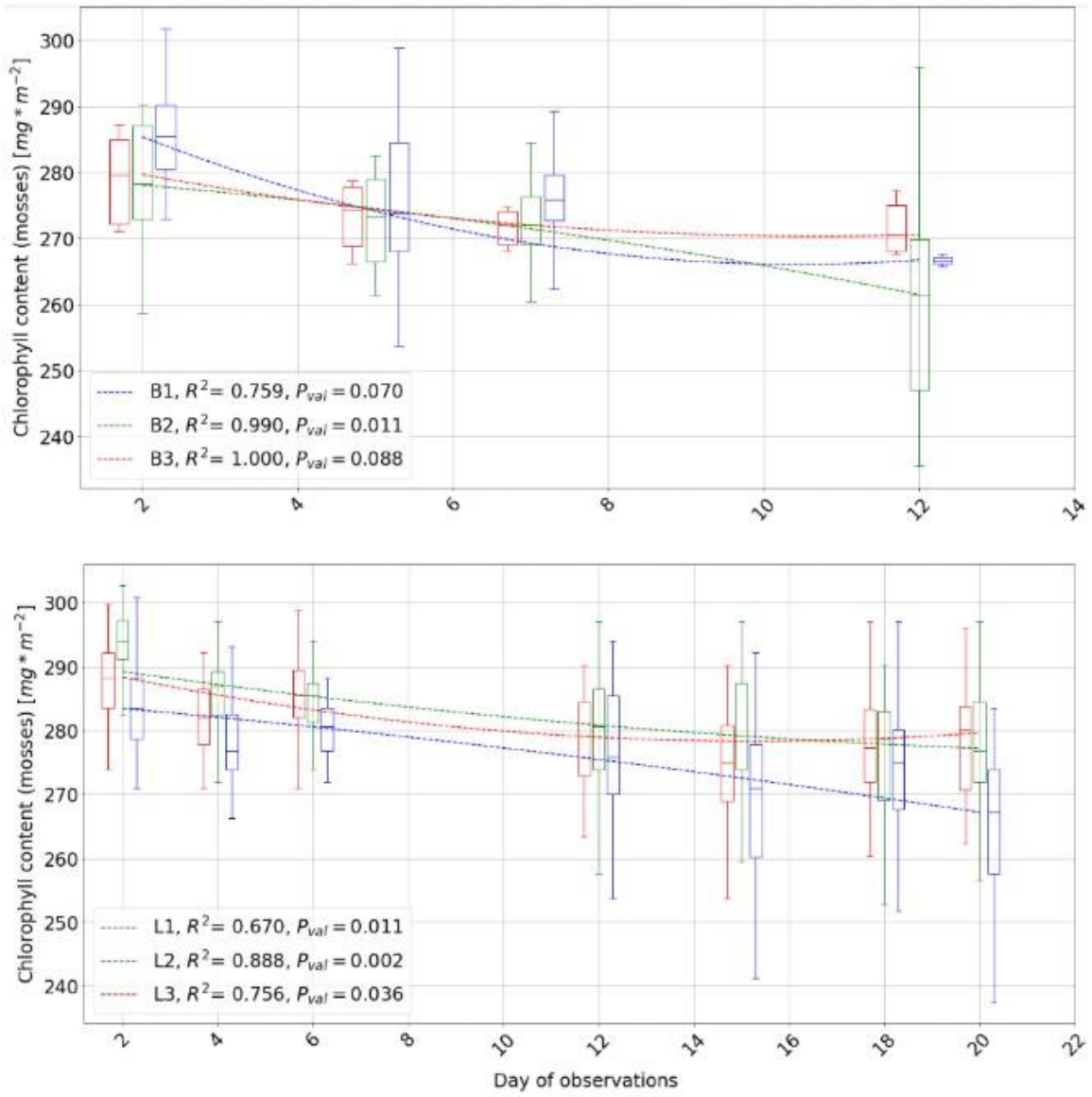

Figure 6. The CC dynamics observed in alkaline fens (**top panel**) and transition mires and quaking bogs (**bottom panel**) habitat samples for mosses layer. Boxes present CC measured in mosses layer in 16 elementary areas. Box edges show 25th and 75th quartile, horizontal line inside the box shows median, whiskers and caps shows all others non-outlier data points.

3.4. BC

Living mosses coverage in transition mire samples decreased in L1 and L3 (from 49% to 0%) and L2 (from 60% to 0%). Changes in herbaceous plants coverage vary between samples. Decrease was identified in L2 (from 46% to 31%) and L3 (from 41% to 40%). The increase was identified in L1 (from 33% to 36%). This sample was dominated by *Eriophorum vaginatum* (Figure 7).

Living mosses coverage in alkaline fens samples decreased in B1 (from 48% to 37%) and B3 (from 58% to 50%). Increase was identified in B2 (from 56% to 57%), where *Campylium* sp. was substituted by *Limprichtia* sp. Changes in herbaceous plants coverage vary between samples. Decrease was identified in B2 (from 42% to 34%) and B3 (from 49% to 22%). No significant change was identified in B1 (fixed at 51%) (Figure 7).

Preprints (www.preprints.org) | NOT PEER-REVIEWED | Posted: 12 December 2018 doi:10.20944/preprints201812.0139.v1

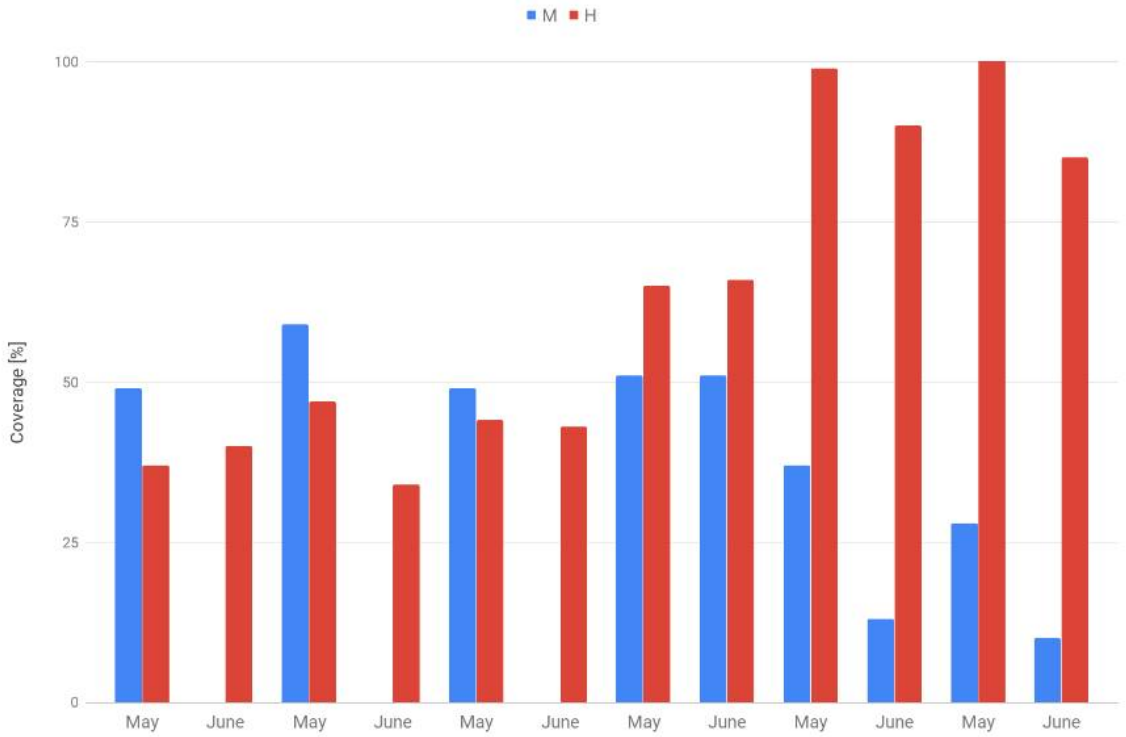

Figure 7. Plant layers' coverage observed in alkaline fens (B) and transition mires and quaking bogs (L) habitat samples (M - moss layer, H - herbaceous layer).

3.5. PLP

In the case of samples for transition mires and quaking bogs, the decrease in the share of pixels classified as living parts of plants in the first phase of the experiment (until around 13th day of observations) is not less than 30 percentage points. A greater decrease in the share of pixels classified as living parts of plants is demonstrated in samples 2 and 3 (a decrease of ca. 40 percentage points) (Figure 8). In the second half of the experiment, the share of pixels classified as living parts of plants slightly increases and then stabilizes to ca. 42% (Figure 8).

In the case of alkaline fens, the change in the share of pixels classified as living parts of plants in the first phase of the experiment (until around 4th day of observations) strongly depends on the sample. The similarity is primarily visible between samples 1 (decrease 28 percentage points) and 3 (decrease 26 percentage points) (Figure 9). Sample 2 shows an increase in the share of pixels classified as living parts of plants associated with the development of *Thelypteris palustris* (increase 20 percentage points) (Figure 8). After reaching a local maximum of ca. 60%, a decrease in is then observed, related to the inhibition of the development of *Thelypteris palustris* and further dying of individuals of the *Carex* sp. (Figure 8).

Preprints (www.preprints.org) | NOT PEER-REVIEWED | Posted: 12 December 2018 doi:10.20944/preprints201812.0139.v1

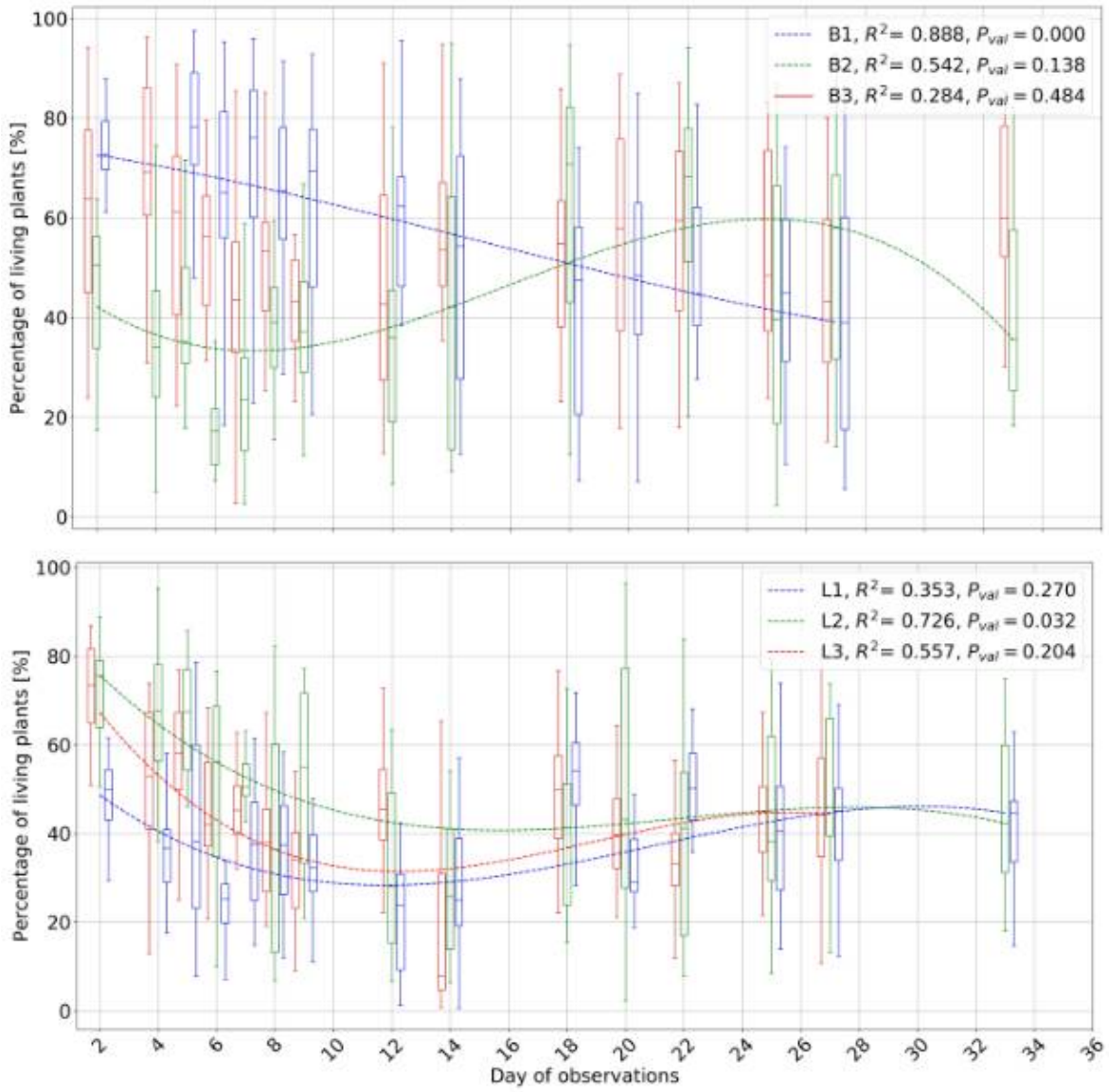

Figure 8. The changes of PLP area observed in alkaline fens (**top panel**) and transition mires and quaking bogs (**bottom panel**) habitat samples. Boxes present percentage of living plants calculated in 16 elementary areas. Box edges show 25th and 75th quartile, horizontal line inside the box shows median, whiskers and caps shows all others non-outlier data points.

3.6. NDVI

NDVI of transition mires and quaking bogs decrease until the 10th day of observations. After the 10th day of observations, the median value of the NDVI was stabilized on level c.a. 0.3. (Figure 9). NDVI of alkaline fens decrease until the 8th day of observations. After the 10th day of observations, the median value of the NDVI was stabilized on level c.a. 0.4 which (Figure 9).

 doi:10.20944/preprints201812.0139.v1

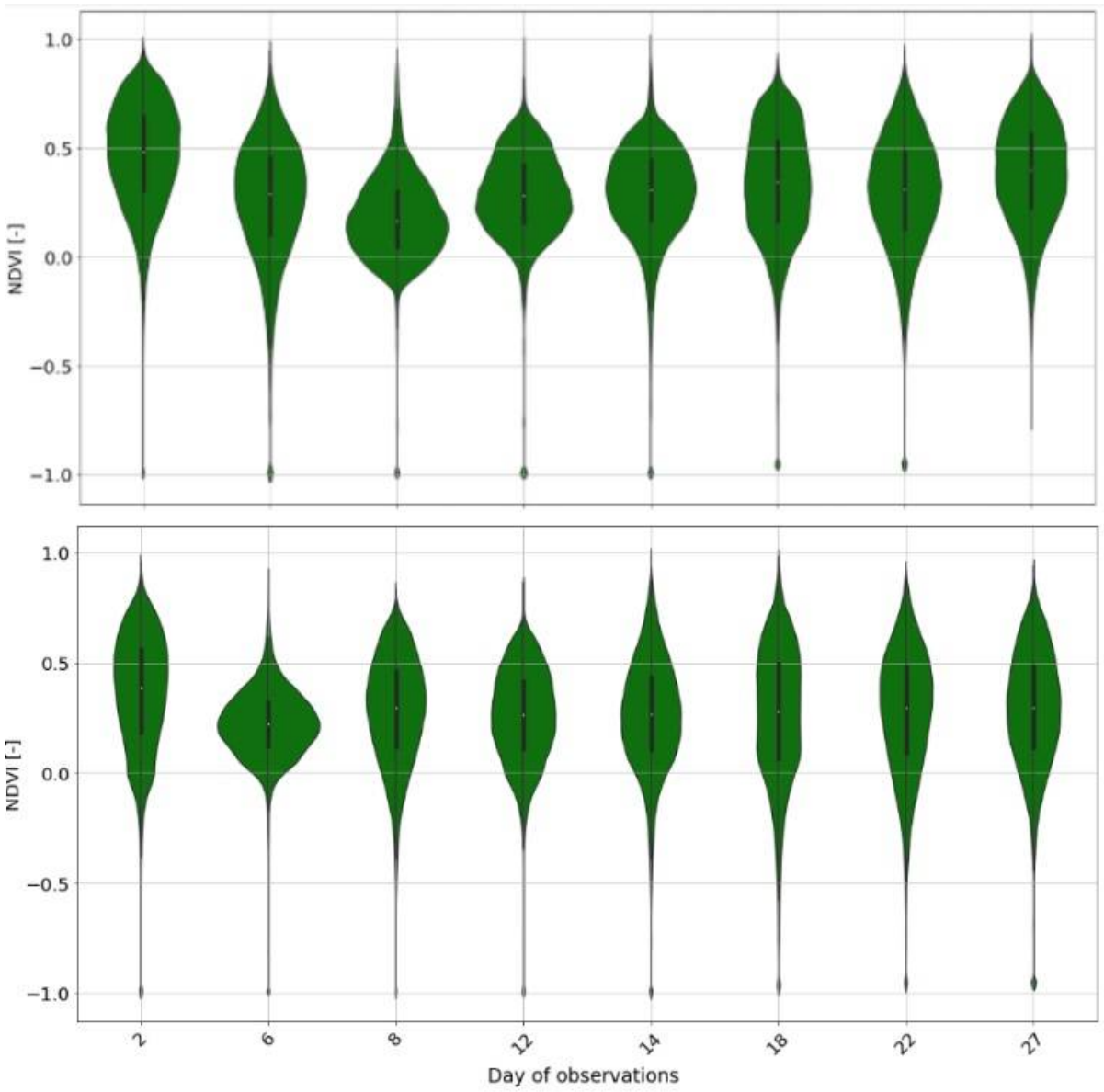

Figure 9. The NDVI dynamics observed in transition mires and quaking bogs (L1 sample presented on **top panel**) and alkaline fens (B2 sample presented on **bottom panel**).

3.7. DT

The decrease in CC, PLP and NDVI in the beginning (from start to the 8th day in case of alkaline fens and to the 10th day in case of transition mires and quaking bogs) of the experiment is related to the high increase of CWSI (Table 1). Linear dependence between VSM and CC can be observed at this step. In a consequence of this, an abrupt in CC of mosses layer is a good indicator of the first phase of desiccation (I DT) (Figure 10).

Later changes in CC, PLP and NDVI are weaker not related to changes in VSM. Depending on the specific plant composition of the sample possible increase of overall plants condition, can be related to the development of plants more resistant to water stress. On the other hand, CWSI is stabilizing around the specific value for each habitat (alkaline fens: 0.15, transition mires and quaking bogs: 0.10). The day-by-day increase in a CWSI value lower than 10% was used as the II DT (Figure 10).

Preprints (www.preprints.org) | NOT PEER-REVIEWED | Posted: 12 December 2018 doi:10.20944/preprints201812.0139.v1

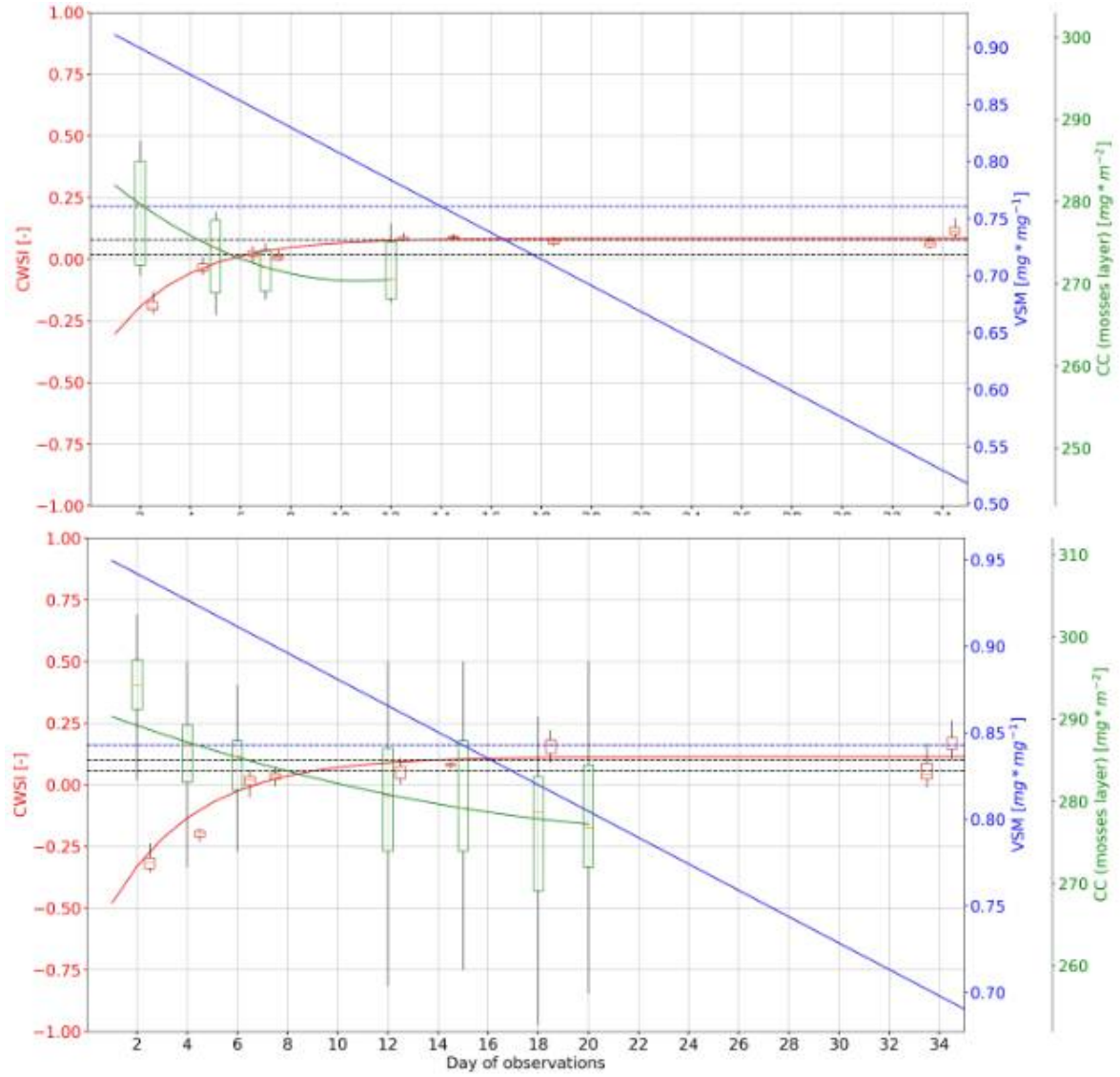

Figure 10. Determination of DT (black dashed lines) and VSMC (blue dashed line) in transition mires and quaking bogs (**top panel**) and alkaline fens (**bottom panel**) samples. Box edges show 25th and 75th quartile, horizontal line inside the box shows median, whiskers and caps shows all others non-outlier data points. Blue solid line shows VSM. Red solid line shows CWSI. Green solid line shows CC.

The I DT in transition mires and quaking bogs (equal to 0) and in alkaline fens (equal to 0.02) represents the initial phase of desiccation (Table 1, Table 2). The II DT equal to 0.12 in transition mires and quaking bogs and 0.08 in alkaline fens represents the phase of drought (Table 1, Table 2).

Table 1. Juxtaposition of analyzed biophysical indicators.

	Alkaline fens				**Transition mires and quaking bogs**			
	IDT value	IDT day	IIDT value	IIDT day	IDT value	IDT day	IIDT value	IIDT day
CC_{MH}	240	7	227	12	-	-	228	20
CC_{M}	273	5	266	12	282	8	275	20
PLP	56	8	40	12	39	10	40	20
NDVI	0,27	6	0,35	12	0,17	8	0,41	18
CWSI	-0,01	5	0,08	10	-0,02	7	0,10	16

[1] MH - mosses and herbaceous plants layer, M - mosses layer.

 doi:10.20944/preprints201812.0139.v1

Table 2. DT determined based on CC and CWSI dynamics

Desiccation phase	Transition mires and quaking bogs	Alkaline fens
Optimum	< - 0.02	< - 0.01
Initial phase of desiccation	- 0.02 - 0.12	- 0.01 - 0.08
Drought	≥ 0.10	≥ 0.08

The obtained results indicate the nonlinear relation of CWSI and habitat condition indicator, which is described by BC. The course of dependence is related to VSM and the strength of this relation decreases as the value of VSM is approaching the VSM_C. CC, PLP and NDVI dynamics at the I phase of desiccation are good indicators, which enable to designate I DT. This is due to the similar dynamics of these quantities in the first phase of desiccation.

4. Discussion

Desiccation thresholds are critical values, which indicate a beginning of two desiccation phases. The first DT refers to the occurrence of symptoms of weakening plants sensitive to water stress. The second DT is associated with deep drainage of the soil.

As a result of the conducted research, it was possible to confirm the issue of the relationship between the land surface temperature with vegetation condition and drying known from the literature [38,39]. Due to the fact that such dependence has never been described before for wetland habitats - transition mires and quaking bogs and alkaline fens - the results should be considered important for the discussion on the possibilities of the widespread use of CWSI. The results of the conducted research indicate the possibility of using CWSI on non-agricultural sites [40, 44]. In this case, it should be understanding as a Habitat Water Stress Index.

The obtained results indicate the diverse sensitivity of wetland habitats to desiccation. Alkaline fens are characterized by approximately constant DT values, regardless of the botanical composition (Figure 3, Table A1). The DT values are much more dependent on the botanical composition in transition mires and quaking bogs. The presence of *Oxycoccus palustris* (sample L2) is associated with an earlier occurrence of desiccation phases. The CWSI dynamics curve in the first phase is characterized by higher steepness.

The different sensitivity of mentioned habitats to desiccation described by the CWSI may be related to the different structure of the mosses layer. In the case of transition mires and quaking bogs, it has a much higher water storage capacity, and therefore the drying rate will be lower than in case of alkaline fens, which results in the later occurrence of DT (Figure 3, Table 1). A longer period of moss vitality is a proof the greater ability to store water in transition mires and quaking bogs than in alkaline fens (Figure 5).

Alkaline fens subject to faster drying early changes the botanical composition. It is associated with the emergence of new plant species germinating from the seed base, better adapted to the new conditions and is illustrated by the increase in the value of CC, PLP and NDVI. This phenomenon is observed in alkaline fens (Table A1).

Weaknesses of the described method include sensitivity to weather conditions when measuring LST among others. Due to the fact that DT and the NWSB are habitat specific, it is recommended for habitats other than transition mires and quaking bogs and alkaline fens to perform similar laboratory experiment.

CWSI may be used in remote sensing wetland communities, allowing identification of areas that require the development of conservation strategy. For this purpose, it is to know DT. In the case of different type of wetland habitat, it is necessary to determine DT. Further research into the use of CWSI in habitats such as transition mires and quaking bogs and alkaline fens may allow the modeling of treatment efficiency in wetlands [45].

5. Conclusions

- Desiccation thresholds are approximately constant for the habitat but could be related to botanical composition.
- The CWSI method developed on the basis of thermal data in the laboratory turned out to be a simple method of assessing the desiccation of wetland habitats based on its biophysical properties. Its universality manifests itself in that it gives a result regardless of the species composition of the habitat.
- CWSI dynamics shows clearly that transition mires and quaking bogs are more vulnerable to the desiccation process, as they have a higher range of CWSI than alkaline fens.
- Application of the described method in different habitat requires DT and NWSB designation.

Author Contributions: Conceptualization, M.G., P.S., M.K., T.G., J.S. and J.C.; Data curation, M.G., W.C., P.S. and J.J.; Funding acquisition, J.C.; Investigation, M.G., W.C., P.S. and J.C.; Methodology, M.G., W.C., P.S., M.K., S.S., T.G., J.S., J.C.; Project administration, J.C.; Resources, M.G., W.C., M.K., J.J. and J.C.; Software, M.G. and W.C.; Supervision, J.C.; Validation, M.G., P.S., M.K., T.G. and J.S.; Visualization, M.G.; Writing – original draft, M.G..; Writing – review & editing, M.G., W.C., P.S., M.K. and S.S.

Funding: This research was funded by the project HabitatARS (BIOSTRATEG2/297915/3/NCBR/2016). The innovative approach supporting monitoring of non-forest Natura 2000 habitats, using remote sensing methods financed by The National Centre for Research and Development.

Conflicts of Interest: The authors declare no conflict of interest

Preprints (www.preprints.org) | NOT PEER-REVIEWED | Posted: 12 December 2018 doi:10.20944/preprints201812.0139.v1

Appendix A

Table 1. Coverage of plant taxons at the beginning and at the end of observations (M - mosses layer, H - herbaceous layer)

	Plant name	L1		L2		L3		B1		B2		B3	
		May	June	May	June	May	June	May	June	May	June	May	June
M	*Sphagnum* sp.	49	-	59	-	49	-	-	-	-	-	-	-
	Campylium sp.	-	-	-	-	-	-	-	-	25	-	-	-
	Limprichtia sp.	-	-	-	-	-	-	51	51	12	13	28	10
H	*Oxycoccus palustris*	-	-	21	17	-	-	-	-	-	-	-	-
	Eriophorum angustifolium	31	32	10	7	13	14	-	-	-	-	-	-
	Carex lasiocarpa	6	8	16	10	31	29	-	-	-	-	-	-
	Agrostis gigantea	-	-	-	-	-	-	1	1	1	-	-	-
	Cardamine amara	-	-	-	-	-	-	2	1	-	-	-	-
	Carex dioica	-	-	-	-	-	-	7	5	-	-	-	-
	Carex diandra	-	-	-	-	-	-	-	-	-	-	10	12
	Carex flava	-	-	-	-	-	-	-	-	6	3	-	-
	Carex lasiocarpa	-	-	-	-	-	-	2	3	-	-	2	7
	Carex panicea	-	-	-	-	-	-	-	-	-	-	14	6
	Carex rostrata	-	-	-	-	-	-	-	-	42	34	8	17
	Comarum palustre	-	-	-	-	-	-	1	1	9	4	12	4
	Thelypteris palustris	-	-	-	-	-	-	-	3	6	15	-	-
	Equisetum fluviatile	-	-	-	-	-	-	3	4	-	-	-	-
	Eriophorum latifolium	-	-	-	-	-	-	-	-	6	3	-	-
	Filipendula ulmaria	-	-	-	-	-	-	5	8	1	-	-	-
	Galium uliginosum	-	-	-	-	-	-	1	2	2	1	2	1
	Geum rivale	-	-	-	-	-	-	-	-	1	-	-	-
	Lysymachia thrysiflora	-	-	-	-	-	-	-	-	3	3	5	10

 doi:10.20944/preprints201812.0139.v1

Menyanthes trifoliata	-	-	-	-	-	-	37	27	-	-	49	27
Phragmites australis	-	-	-	-	-	-	-	-	5	5	-	-
Salix rosmarinifolia	-	-	-	-	-	-	5	9	17	22	5	-
Stachys palustris	-	-	-	-	-	-	1	2	-	-	-	-
Salix cinerea	-	-	-	-	-	-	-	-	-	-	-	1

References

1. Petrasovits, I. General review on drought strategies*; Transactions of 14th Congress on Irrigation and Drainage*, Vol. I-C, International Commission on Irrigation and Drainage, Rio de Janeiro, 1990; pp 1–12.
2. Brandyk, T.; Szatyłowicz, J.; Oleszczuk, R.; Gnatowski, T. Water-related physical attributes of organic soils; In *Organic soils and peat materials for sustainable agriculture*; Parent, L.E.; Ilnicki, P. Eds.; Boca Raton: CRC Press and International Peat Society, 2002; pp. 33–66.
3. Hsieh, I.; Gill, A.; Finzi, A.; Response of surface CH4 and CO2 fluxes to whole ecosystem warming and elevated CO2 in a boreal black spruce peatland, northern Minnesota; *American Geophysical Union*, 2017; Available online: http://adsabs.harvard.edu/abs/2017AGUFM.B42C..03H (accessed on 27 August 2018).
4. Lohila, A.; Aurela, M.; Hatakka, J.; Tuovinen, J.; Penttila, T.; Laurila, T. Long-term GHG measurements at a northern boreal fen show stable CH4 emissions, increasing soil respiration and endangered carbon uptake as climate is warming; *20th EGU General Assembly*, EGU2018, Proceedings from the conference 4-13 April, Vienna, Austria, 2018; p.15163.
5. Hongjun, W.; Richardson, C.; Mengchi, H. Dual controls on carbon loss during drought in peatlands. *Nature Clim. Change* 2015, 5, 584–587.
6. Grygoruk M., Okruszko T., Do water management and climate-adapted management of wetlands interfere in practice? Lessons from the Biebrza Valley, Poland. *Wetlands Water Fram. Dir*. 2015; pp. 53–67.
7. Lewis, R.; Milbrandt, E.; Brown, B.; Krauss, K.; Rovai, A.; Beever, J.; Flynn, L. Stress in mangrove forests: Early detection and preemptive rehabilitation are essential for future successful worldwide mangrove forest management. *Marine Pollut. Bull*. 2016, 109, 764–771.
8. Fay, P.; Guntenspergen, G.; Olker, J.; Johnson, W. Climate change impacts on freshwater wetland hydrology and vegetation cover cycling along a regional aridity gradient. *Ecosphere* 2016, 7, 1-12.
9. Zedler, J.; Kercher, S. Causes and consequences of invasive plants in wetlands: opportunities, opportunists, and outcomes. *Crit. Rev. Plant Sci*. 2004, 23, 431–452.
10. Spinoni, J.; Vogt, J.; Naumann, G.; Barbosa, P.; Dosio, A. Will drought events become more frequent and severe in Europe?. *Int. J. Clim*. 2018, 38, 1718–1736.
11. Bąk, B.; Łabędzki, L. Prediction of precipitation deficit and excess in Bydgoszcz Region in view of predicted climate changes. J. *Water Land Dev.* 2014, 23 (X–XII): 11–19, DOI: 10.1515/jwld-2014-0025
12. Bachmair, S.; Stahl, K.; Hannaford, J.; Acreman, M.; Svoboda, M.; Knutson, C.; Smith, K.; Wall, N.; Fuchs, B.; Crossman, N.; Overton, I. Drought indicators revisited: the need for a wider consideration of environment and society. *Wiley Interdisc. Rev.: Water* 2016, 3, 516–536.
13. McKee, T.; Doesken, N.; Kleist, J. The relationship of drought frequency and duration to time scales; *Proceedings of the 8th Conference of Applied Climatology*, 17-22 January, Anaheim, California, 1993; pp. 179–184.
14. Bloomfield, J.: Marchant, B. Analysis of groundwater drought building on the standardised precipitation index approach. *Hydrol. Earth Syst. Sci*. 2013, 17, 4769–4787.
15. Paulo, A.; Pereira, L.; Matias, P. Analysis of local and regional droughts in southern Portugal using the theory of runs and the Standardised Precipitation Index. In Rossi, G.; Cancelliere, A.; Pereira, L.S.; Oweis, T.; Shatanawi, M.; Zairi, A. eds. Tools for Drought Mitigation in Mediterranean Regions. *Water Science and Technology Library*, Volume 44, Springer, Dordrecht, 2003.
16. Guenang G., Kamga F., Computation of the Standardized Precipitation Index (SPI) and Its Use to Assess Drought Occurrences in Cameroon over Recent Decades. *J. Appl. Meteor. Climatol.* 2014, 53, 2310–2324.

17. Łabędzki, L.; Bąk, B. Meteorological and agricultural drought indices used in drought monitoring in Poland. *Meteorol. Hydrol. Water Manag.* 2014, 2, 3–13.
18. Morid, S.; Smakhtin, V.; Moghaddasi, M. Comparison of seven meteorological indices for drought monitoring in Iran. *Int. J. Climatol.* 2006, 26, 971–985.
19. Do-Woo, K.; Hi-Ryong, B.; Ki-Seon, C. Evaluation, modification, and application of the Effective Drought Index to 200-Year drought climatology of Seoul, Korea. *J. Hydrol.* 2009, 378, 1–12.
20. Deo, R.; Sahin, M. Application of the extreme learning machine algorithm for the prediction of monthly Effective Drought Index in eastern Australia. *Atmos. Res.* 2015, 153,
21. Łabędzki, L.; Bąk, B. Standardized climatic water balance as an indicator of drought. *Acta Agroph.* 2004, 3, 117–124. [In Polish]
22. Łabędzki, L.; Bąk, B. The method of index assessment and classification of soil moisture in permanent grasslands in Poland. *Infrastruktura i Ekologia Terenów Wiejskich* 2015, 3, 515–531. [In Polish]
23. Gardner, B.: Nielsen, D.; Shock, C. Infrared thermometry and the crop water-stress index. 1. History, theory, and base-lines. *J. Prod. Agric.* 1992, 5, 462–466.
24. Hunt, E.; Hubbard, K.; Wilhite, D.; Arkebauer, T.; Dutcher, A. The development and evaluation of a soil moisture index. *Int. J. Climatol.* 2009, 29, 747–759.
25. Vicente-Serrano, S.; Begueria, S.; Lorenzo-Lacruz, J.; Camarero, J.; Lopez-Moreno, J.; Azorin-Molina, C.; Revuelto, J.; Moran-Tejeda, E.; Sanchez-Lorenzo, A. Performance of drought indices for ecological, agricultural, and hydrological applications. *Earth Interact.* 2012, 16, 1–27.
26. Amazirh, A.; Er-Raki, S.; Chehbouni, A.; Rivalland, V.; Diarra, A.; Khabba, S.; Ezzahar, J.; Merlin, O. Modified Penman-Monteith equation for monitoring evapotranspiration of wheat crop: Relationship between the surface resistance and remotely sensed stress index. *Biosyst. Eng.* 2017, 164, 68–84.
27. DeJonge, K.; Taghvaeian, S.; Trout, T.; Comas, L. Comparison of canopy temperature-based water stress indices for maize. *Agric. Water Manag.* 2015, 58, 51–62.
28. Sayago, S.; Ovando, G.; Bocco, M. Landsat images and crop model for evaluating water stress of rainfed soybean, *Remote Sens Environ.* 2017, 198, 30–39.
29. Karaca, C.; Tekeliogliu, B.; Byuktas, D.; Bastug, R. Relations between Crop Water Stress Index and stomatal conductance of soybean depending on cultivars, Fresen. *Environ. Bull.* 2018, 27, 4212–4219.
30. Sezen, S.; Yazar, A.; Dasgan, Y.; Yucei, S.; Akyilidiz, A.; Tekin, S.; Akhoundnejad, Y. Evaluation of Crop Water Stress Index (CWSI) for red pepper with drip and furrow irrigation under varying irrigation regimes. *Agric. Water Manag.* 2014, 143, 59–70.
31. Colak, Y.; Yazar, A.; Colak, I.; Akca, H.; Duraktekin, G. Evaluation of Crop Water Stress Index (CWSI) for Eggplant under varying irrigation regimes using surface and Subsurface Drip Systems. *Agric. Agric. Sci. Proc.* 2015, 4, 373–382.
32. Bahmani, O.; Sabziparvar, A.; Khosravi, R. Evaluation of yield, quality and crop water stress index of sugar beet under different irrigation regimes. *Water Sci. Technol.: Water Supp. 2016*, 17, 571–578.
33. Bellvert, J.; Zarco-Tejada, P.; Girona, J.; Fereres, E. Mapping Crop Water Stress Index in a 'Pinot-noir' vineyard: comparing ground measurements with thermal remote sensing imagery from an unmanned aerial vehicle. *Precision Agricult.* 2014, 15, 361–376.
34. Egea, G.; Padilla-Diaz, C.; Martinez-Guanter, J.; Fernandez, J.; Perez-Ruiz, M. Assessing a Crop Water Stress Index derived from aerial thermal imaging and infrared thermometry in super-high density olive orchards. *Agricult. Water Manage.* 2017, 187, 210–221.
35. Park, S.; Ryu, D.; Fuentes, S.; Chung, H.; Hernandez-Montes, E.; O'Connel, M. Adaptive estimation of Crop Water Stress in nectarine and peach orchards using high-resolution imagery from an unmanned aerial vehicle (UAV). *Remote Sens.* 2017, 9, 826.
36. Virlet, N.; Lebourgeois, V.; Marinez, S.; Costes, E.; Labbe, S.; Regnard, J. Stress indicators based on airborne thermal imagery for field phenotyping a heterogeneous tree population for response to water constraints, *J. Exp. Bot.* 2014, 65, 5429–5442.
37. Matese, A.; Di Gennaro, F. Practical applications of a multisensor UAV Platform based on multispectral, thermal and RGB high resolution images in precision viticulture. *Agric.* 2018, 8, 116.
38. Taghvaeian S.; Chávez J.L.; Hansen N.C. Infrared thermometry to estimate crop water stress index and water use of irrigated maize in Northeastern Colorado. *Remote Sens.*, 4(11), 2012, 3619-3637.
39. Taghvaeian, S.; Chávez, J.; Altenhofen, J.; Trout, T.; DeJonge, K. Remote sensing for evaluating crop water stress at field scale using infrared thermography: Potentials and limitations. *Hydrol. Days* 2013, 4, 74–83.

40. Ciężkowski, W.; Jóźwiak, J.; Szporak-Wasilewska, S.; Kleniewska, M.; Gnatowski, T.; Dąbrowski, P.; Góraj, M.; Szatyłowicz, J.; Ignar, S.; Chormański, J. UAV Based Crop Water Stress Index for Wetland Habitats. *Preprints* 2018, 2018100389 (doi: 10.20944/preprints201810.0389.v1).
41. Bellvert, J.; Marsal, J.; Girona, J.; Zarco-Tejada, P.J. Seasonal evolution of crop water stress index in grapevine varieties determined with high-resolution remote sensing thermal imagery. *Irrig. Sci*. 2015, 33, 81–93.
42. Dierschke, H. Pflanzensoziologie – Grundlagen und Methoden; Ulmer: Stuttgart, 1994.
43. Akaike, H. Information theory and an extension of the maximum likelihood principle. In Parzen, E.; Tanabe, K.; Kitagawa, G. Eds. *Selected papers of Hirotugu Akaike. Springer Series in Statistics (Perspectives in Statistics)*, Springer, New York, NY, 1988.
44. Ciężkowski, W.; Jóźwiak, J.; Szporak-Wasilewska, S.; Dąbrowski, P.; Kleniewska, M.; Góraj, M.; Chormański, J. Water Stress Index for Bogs and Mires Based on UAV Land Surface Measurements and Its Dependency on Airborne Hyperspectral Data. *In IGARSS 2018-2018 IEEE International Geoscience and Remote Sensing Symposium IEEE*, 2018, 9257-9260.
45. Hui, Z.; Qing-wei, Z.; Bai-xing, Y.; Yin-xiu, L.; Xiang-fei, Y.; Yoram, G.; Xian-wei, C. Influence of vegetation type and temperature on the performance of constructed wetlands for nutrient removal. *Water Sci. Techn.* 2018, 77, 829–837.